SULFUR DISPERSION QUANTITATIVE ANALYSIS IN ELASTOMERIC TIRE FORMULATIONS BY USING HIGH RESOLUTION X-RAY COMPUTED TOMOGRAPHY

DAYAKAR PENUMADU,[1,*] JUN-CHENG CHIN,[1] STEPHEN YOUNG,[1] FREDERICK IGNATZ-HOOVER,[2] TOM FLOYD,[2] PETER CHAPMAN[3]

[1] TICKLE COLLEGE OF ENGINEERING AND JOINT INSTITUTE FOR ADVANCE MATERIALS, 327 JOHN D. TICKLE BUILDING, 851 NEYLAND DRIVE, UNIVERSITY OF TENNESSEE, KNOXVILLE, TN 37996
[2] TIRE ADDITIVES TECHNOLOGY DIVISION, 260 SPRINGSIDE DRIVE, EASTMAN CHEMICAL COMPANY, AKRON, OH 44333
[3] MATERIALS ANALYSIS LAB, 100 EASTMAN ROAD, EASTMAN CHEMICAL COMPANY, KINGSPORT, TN 37660

RUBBER CHEMISTRY AND TECHNOLOGY, Vol. 94, No. 4, pp. 626–641 (2021)

ABSTRACT

Good dispersion of compounded ingredients in a rubber formulation is important for mechanical performance. After mixing, certain materials can remain undispersed within the rubber matrix, which could lead to critical flaws, influencing performance according to the Griffith failure criteria. High resolution X-ray computed tomography (XCT) offers a unique opportunity to measure phase domain size and distributions. Fillers such as carbon black or silica can be differentiated from sulfur or zinc oxide, providing an opportunity to determine dispersion characteristics of the various phases. The XCT technique has become an important characterization tool for three-dimensional and higher dimension material science due to the availability of polychromatic micro-focus X-ray sources and efficient high spatial resolution detectors with superior scintillators. High resolution XCT provides very rich data quantifying mixing efficiency of particulates in a matrix, such as insoluble sulfur or silica particles in rubber. Imaging with X-rays provides attenuation, phase, or scattering contrast and will prove to be a critical method for evaluating the field of rubber crosslinking, considering realistic environments in situ. This paper highlights methodology development and validation and provides insight on the dispersion of polymeric (insoluble) sulfur in rubber formulations. Dispersion assessment is compared using three techniques: high resolution XCT, population survival analysis in tensile testing, and optical microscopy. [doi:10.5254/rct.21.79997]

INTRODUCTION

Dispersion of ingredients during compounding in rubber is important for ideal mechanical properties, because polymers, fillers, and various rubber additives require good dispersion to ensure high performance. Poor dispersion, resulting from inadequate mixing or inherently large particle-sized materials, can lead to reduced performance of various mechanical properties such as tensile and tear properties, fatigue life, and abrasion resistance.[1–7] Fine powdery additives such as accelerators, zinc oxide, and insoluble sulfur (IS) and fillers such as carbon black and precipitated silica are characteristically difficult to disperse.[8–16] Ineffective filler dispersion, in general, can lead to mechanical flaws due to the solid, undispersed materials, whereas ineffective curative dispersion could generate non-homogeneous networks characterized by areas of high crosslink density capable of behaving as critical flaws in the compound.

One of the most common problems of rubber manufacturing is achieving uniform dispersion of ingredients in rubber. The causes for poor dispersion are typically due to one or some combination of the following: poor-quality materials, off-spec materials, agglomeration and compaction of materials, improper order in which ingredients are mixed, improper mixing, and equipment problems. Fine powdery materials such as fine particle fillers, curatives, or IS are characteristically difficult to disperse. In poorly mixed compounds, larger aggregates of powders or inherently large particles fail to disperse and can be observed as “spots” or powder-aggregates in the compound by optical or scanning electron microscopy (SEM). The solutions to dispersion problems include use

---

[*] Corresponding author. Ph: (865) 974-7708; email: dpenumad@utk.edu

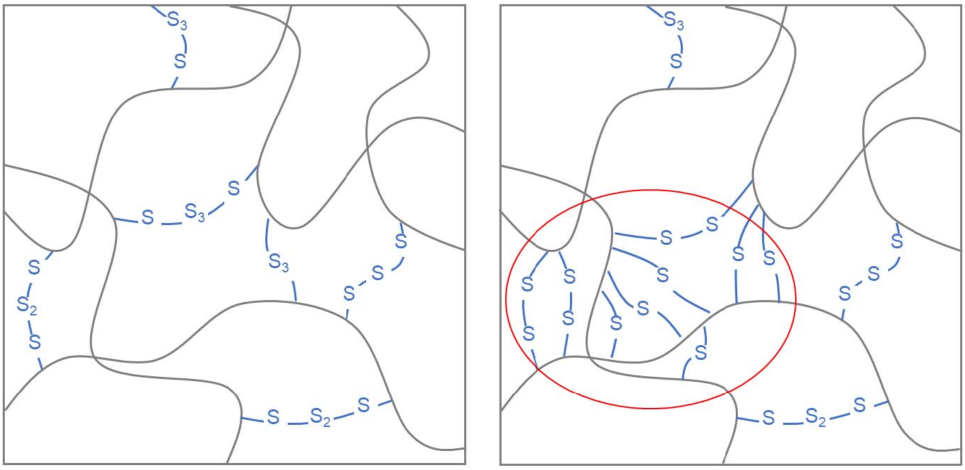

FIG. 1. — Schematic of good dispersion of IS in polymer matric (left) and poor dispersion, causing localized areas of high crosslinked density (right).

of high-quality materials, mixing cycle modifications, or improved dispersion properties of the materials and or improved mixing equipment.

Transient inclusions are defined herein as inclusions of transient materials that will be transformed upon chemical conversion such as vulcanization. Permanent inclusions form as poorly dispersed solids (especially fillers) within the elastomer or form as voids when an elastomer cracks or delaminates from the surface of poorly dispersed solid particles.[5] Transient inclusions form as materials transform from discrete phases of undispersed solid materials to in-homogeneous or semi-continuous single phase solids. Curatives, accelerators, and activating chemicals must be fully dissolved and of uniform concentration throughout the component as vulcanization progresses to generate a network of uniform crosslink density. During vulcanization, polymeric IS depolymerizes to cyclo-octasulfur that dissolves and diffuses throughout the component.[17] Accelerator, zinc oxide, and stearic acid must also dissolve and react, forming a zinc accelerator complex that, in turn, interacts with the sulfur-forming active sulfurating intermediates.[18] The intermediates react with the polymer to attach sulfur, forming a sulfurated polymer and then eventually a crosslink. High concentrations of the sulfurating intermediate can occur in the loci of large particles or aggregates of undispersed sulfur as the cyclo-octasulfur dissolves into the compound. Consequently, when the rate of vulcanization is faster or competitive with the rate of diffusion, regions of high crosslink density form (Figure 1) around or near to the undispersed aggregates. These highly crosslinked localized regions may exhibit severe tensile strength gradients that, under sufficient strain energy density, behave as critical flaws. A direct characterization method to visualize and quantify the dispersion of fillers and other compounding ingredients including IS before vulcanization reaction would benefit predictive capability of related mechanical performance.

Dispersion can be assessed in multiple ways with various levels of accuracy and sensitivity including tensile and X-ray computed tomography (XCT) characterization techniques. Tensile strength and elongation decreased with increasing particle size of various accelerators; higher melting accelerators were more sensitive to these effects.[19,20] The application of two-parameter Weibull distributions and population survival statistics to the tensile strength of cured rubber provides a somewhat quantifiable yet indirect technique to evaluate IS dispersion.[17] The Weibull scale and shape estimates can be used as key parameters to characterize and compare the quality of dispersion in rubber. Although tensile testing of large populations of samples is labor intensive, this technique samples larger volumes than two-dimensional (2D) imaging techniques, providing a better representation of dispersion, especially for marginally dispersed materials.

Knowing crack or critical flaw sizes and population statistics is critical to understanding fracture mechanics of a material according to Wöhler or Griffith criteria.[1,6,21] Robin and Alshuth have shown how XCT can be used as a non-destructive technique to characterize cracks (voids) or silica filler flaws, both characteristically high X-ray contrast situations, inside an elastomeric sample. They have further demonstrated how understanding flaw size distributions leads directly to determination of Wöhler S-N type curves. Robin and Alshuth also discussed the sample volume problem in the analysis of low frequency defects in mechanical testing; that is, testing small volumes of materials may fail to detect presence of the flaws when defects are of low volume and small size and/or frequency.[22] Using the XCT technique combined with Weibull survival population statistics, the critical flaw size for poorly dispersed silica for tensile failure in a silica-filled tread compound was estimated to be on the order of 75 μm.[23]

The 2D imaging techniques such as optical microscopy and SEM offer more direct assessment of dispersion. Optical imaging often relies on image gray scale contrast to define particle size and particle size distributions. Consequently, in carbon-filled rubber compounds, optical imaging cannot discriminate between inclusions caused by accelerators, sulfur, zinc oxide, or other "light-colored" materials. In white-filled compounds, even the observations of light-colored materials can be virtually impossible. The SEM techniques coupled with a secondary technique such as energy dispersive X-ray spectroscopy (EDS) are atom specific and offer a direct characterization of material dispersion. Either technique requires very large surface areas, imaged at high resolutions to achieve the sensitivity afforded by the tensile dispersion technique. The 2D image analysis sampling quality and efficiency limit the efficacy of these techniques, whereas previous three-dimensional (3D) imaging by XCT has only been demonstrated for high-contrast hetero-phase materials. Herein, we developed a robust and precise, non-invasive characterization procedure using micro-focus optics–based XCT to evaluate the 3D visualization and quantification of compounding ingredients of intermediate X-ray contrast including insoluble sulfur products before vulcanization.

EXPERIMENTAL

OPTICAL IMAGING INSTRUMENT SETUP

A VHX-6000 optical microscope (Keyence, Itasca, IL, USA) with VHX software was used in developing the optical dispersion test. This digital microscope has an expanded XYZ motorized travel range with 2D and 3D image-stitching capability up to a 10 cm × 10 cm sample surface. Autofocusing capability allows for prompt imaging of a sample surface. The high-performance zoom lens (VH-Z20T; Keyence, Itasca, IL) has 20–200× magnification capability, but for practicality, the current test method uses only 30× magnification and the 2D-XY motorized movement. A polarization filter has been added to the end of the Z20 lens to filter out light specifically reflected from non-crystalline materials. Green rubber samples were prepared using a standard clicker-die cutting press. Appropriate dies had the following dimensions: double 76.2 mm × 76.2 mm square die and a parallel 101.6 mm blade steel rule die, which yielded eight 1 cm strips. Particle enumeration and size quantification were processed using JMP Statistical Data Processing Software from SAS Institute (Cary, NC, USA).

XCT INSTRUMENTAL SETUP

Digital XCT was performed using a custom-developed laboratory Siemens (In Vitro; Siemens, Knoxville, TN) micro-focus–based source (maximum energy of 130 KeV with fine spot size of 5

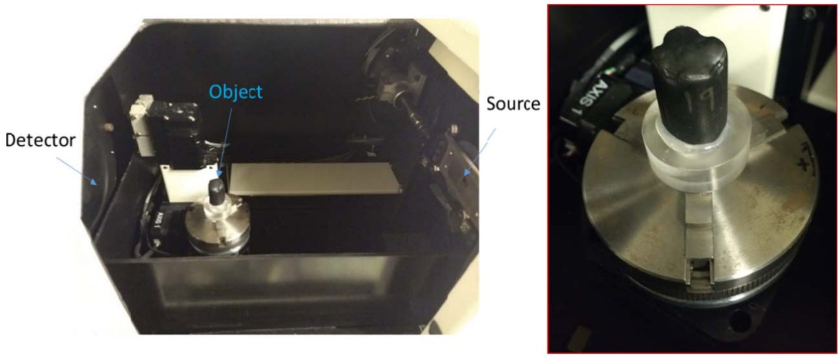

FIG. 2. — XCT setup inside the shielded cabinet and rubber sample.

μm) and a high resolution scintillator–based flat panel detector (Figure 2). The source-to-object distance and the source-to-detector distance (Figure 3) define the geometric magnification for a given location of the object (rubber composite sample in this study). Micro-computed tomography (micro-CT) systems have the flexibility for providing relatively large field of view (FOV) and high spatial resolution, limited typically by the source spot size, which is adequate for studying the dispersion of IS at length scales on the order of a few micrometers. The X-rays generated by the micro-focus source diverge at an angle, providing a cone-beam; thus, samples can be imaged at various geometric magnifications by moving the sample close to the source to provide high resolution measurements or close to the detector to provide low resolution measurements. Use of adequate spatial resolution is required to visualize and quantify the dispersion nature of the two types of IS considering the trade-off between spatial resolution and FOV and target particle size range of interest. Using the 3D visualization and analysis software packages called Simpleware®, reconstructed 2D slices containing the attenuation information were evaluated to visualize and quantify target phases of interest in the rubber compounds corresponding to IS.[24,25]

$$Magnification = \frac{SDD}{SOD}$$

$$Image\ Pixel\ Size = \frac{Detector\ Pixel\ Size}{Magnification}$$

SDD: Source to Detector Distance

SOD: Source to Object Distance

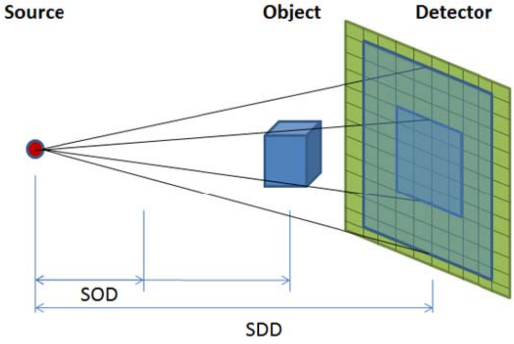

FIG. 3. — Image pixel size and geometric magnification.

TABLE I
MB FORMULATION

Component	Pass 1, phr	Pass 2, phr
NR TSR 10	100	
N339 carbon black	50	
Stearic acid	2	
Zinc oxide	8	
N-Phenyl-*N′*-(1,3-dimethylbutyl)-*p*-phenylene-diamine	2	
Pass 1 compound		162
Total parts	162	162

RUBBER SAMPLE PREPARATION

Rubber was formulated following the tensile dispersion protocol.[17] A rubber masterbatch (MB) was prepared at Chem Technologies, Ltd. (Middlefield, OH, USA). Procedure and ingredients are listed in Table I. Rubber should rest overnight between the first and second pass. Final rubber specification requires a Mooney viscosity (M_{1+4}) of <81. The MB is normally aged 4 to 6 weeks before use. This allows for the initial Mooney viscosity to reach a minimum of 150 or greater.

The IS mix was prepared in a Banbury 1.5 L tangential mixer followed by two passes through a two-roll mill (no banding). The protocol for weighing components for the IS mix is described in Tables II and III. The final mix involves the addition of MB, dicyclo-2-benzothiazole sulfenamide (DCBS), and IS. The IS may contain 10 or 20% oil, and actual weights on all components are adjusted to equal sulfur content. Mixing conditions included operating the Banbury mixer at 35 rpm and controlling temperature control unit water temperature to 68.3 °C. Ram pressure was set at 413.69 kPa. Total mixer time once the mixer door is down is exactly 85 s. Actual rubber temperature at the end of the mixing cycle is generally 71.1–73.8 °C.

SAMPLE PREPARATION OF MILLED RUBBER SAMPLE SUBMITTED FOR OPTICAL IMAGING

Two sheets were prepared that were ~76 mm × 76 mm and 4.6 mm in thickness. The samples were placed in a freezer set at below 0 °C overnight (>12 h). This freezing step is critical to prevent smearing of dispersed IS during cutting the sample. Immediately after removing samples from the freezer, they are cut into strips by using the clicker-die. Each strip was rotated 90°. Strips were

TABLE II
CALCULATION FOR IS (OT20) CURATIVE MIXING FORMULATION

Component	Calculated value
MB, phr	162.0
DCBS, phr	1.0
IS, phr	6.3
Total, phr	169.3
Banbury mix vol, mL	1500
Fill factor, %	74
Specific gravity, g/mL	1.14

TABLE III
INPUTS FOR REPLICATE WEIGHTS (IN GRAMS) FOR OT10 AND OT20 IS FORMULATIONS

% Sulfur	MB	DCBS	Sulfur	Total
90	1217.4	7.5	41.8	1266.7
80	1212.4	7.5	46.8	1266.7

pressed together. The cut surfaces facing up were imaged (Figure 4). Image acquisition occurred within 5 min after the sample preparation to avoid inaccuracies.

SAMPLE PREPARATION OF MILLED RUBBER SAMPLE SUBMITTED FOR XCT IMAGING

Cylindrical formulated rubber samples were prepared as described above for sheet samples, except that sheets were milled to ~1.5 mm thickness and trimmed to a width of 3.2 cm. When rolled into a cylindrical button, the rubber had a diameter of 1.9 cm. To remove air pockets and form a solid specimen, the samples were placed in a standard type mold and pressed to 75 tons at room temperature.[26] The final specimen dimensions had a cylindrical diameter of 1.6 cm and a height of 1.8 cm.

SAMPLE PREPARATION FOR POPULATION SURVIVAL ANALYSIS

Tensile experiments were conducted according to ASTM Standard D-412 protocols. Samples were cured in 152.4 mm × 152.4 mm slabs with a nominal thickness of 1.65 mm. Tensile sheets were cured at 170 °C for the time determined by the moving die rheometer rheometer to reach maximum torque at 170 °C. Dumbbell-shaped tensile samples (50 per mix) are died using Die C as described in ASTM Standard D-412 and then tested accordingly.

SEM OF SULFUR MATERIALS

The microstructure of two sulfur materials were examined using a variable pressure scanning electron microscope (model EVO MA15, Carl Zeiss, Wetzlar, Germany) at an accelerating voltage of 20 kV. The atomic constituents of the sulfur were measured using EDS.

X-RAY RADIATION BASED NON-INVASIVE IMAGING

To visualize the dispersion of compounding ingredients in rubber such as polymers, fillers, and various additives in the interior of a sample, an imaging technology has been developed using X-ray

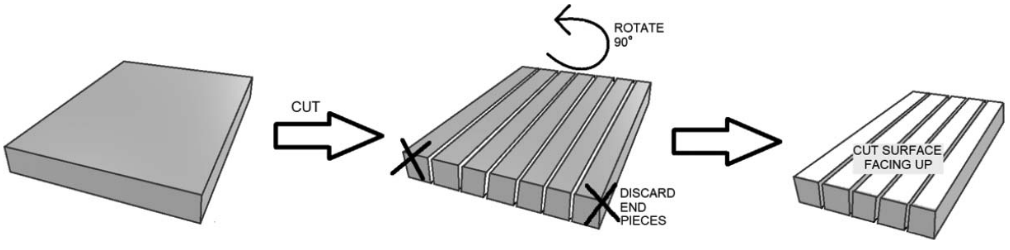

FIG. 4. — Cartoon depicting sectioning and orientation of prepared rubber specimens for Keyence optical image analysis.

micro-CT with a custom-developed experimental setup. Until recently, dispersion assessment in elastomeric materials has been obtained by destructive techniques such as sectioning of samples, subsequent careful polishing, and 2D images from optimal microscopy followed by digital image analysis.[27] XCT was used in this study as an alternative approach. Lab-based micro-CT machines are readily available and provide resolutions of <1 μm, with the highest resolution achievable at synchrotron imaging facilities.[28–30] Current trends also are facilitating the integration of tomography imaging experiments coupled with in situ mechanical loading tests.[31,32] It is essential to choose appropriate energy of the photons and FOV and spatial resolution for matching the length scales of interest, in this study targeting particle and agglomerate sizes of IS after compounding process.

When X-ray beams pass through a sample, some of them are attenuated (scattered or absorbed). The amount of attenuation is characterized by the attenuation coefficient (μ) which is a function of the material type largely influenced by the atomic number of elements contained in the given pixel (2D images) or in a given voxel (3D images) and the energy of the x-rays passing through the material. The attenuation process is linear and can be presented as the Lambert–Beer's law for monochromatic beam as in Eq. 1, where I_0 is the incident beam intensity and I is the beam intensity after passing the material:

$$I = I_0 e^{-\int \mu(x)dx} \tag{1}$$

The CT experiment is performed by taking several projections at different angular positions of the sample. All projections can be put together, resulting in a reconstructed tomography slice that shows the spatial distribution of the attenuation value in the interior of the sample. The reconstruction is commonly done with an algorithm such as filtered back-projection as well as iterative algorithms. The given samples were rotated 360°, with appropriate number of projections for tomography by using suitable energy that accentuates distinct attenuation values for IS compared with matrix MB rubber material and other additives described above. These images were reconstructed by using the filtered back-projection algorithm using Octopus software.[33–38] The X-rays interact with the electron cloud of an atom; as a result, the X-rays' cross sections (attenuation) increase with the atomic number. Details on the background and technique as applied to studying composite materials can be found in Penumadu et al.[25]

TWO-PARAMETER WEIBULL SURVIVAL STATISTICAL ANALYSIS FOR ULTIMATE STRENGTH

The population distributions of sample failures can be described by a probability distribution, and there are many available types of distributions. Weibull distributions are commonly used in many time-to-fail applications, such as understanding fatigue life, patient survival, and strength of dental materials.[39–41] In this case, we are substituting tensile strength at break, T_b, as the time parameter for the distribution. The values of T_b among a population of samples are assumed to have a shape consistent with the two-parameter Weibull distribution (Figure 5). The Weibull survival curve is used to visualize performance of tested material that follows a Weibull distribution (Figure 6). The curve illustrates the probability of survival across T_b levels, where the distance above the curve at a given tensile strength describes the proportion of samples that have failed and the distance below the curve at a given T_b represents the proportion that have survived testing. The two-parameter Weibull distribution is characterized by a scale parameter alpha (which in this case is T_b) and a shape parameter beta, also known as α and β, respectively, and can take on many different shapes depending on the values of those parameters. These parameters are estimated from data using statistical software by maximum likelihood estimation, an estimation method that finds the most likely distribution parameters given the observed tensile measurements. The α parameter

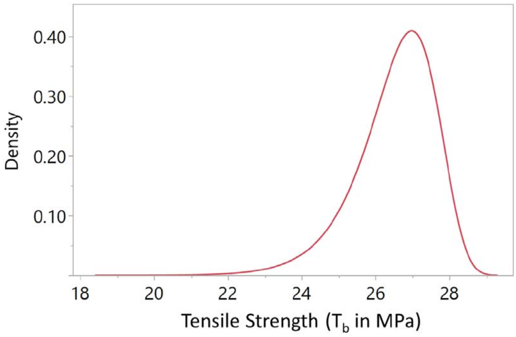

FIG. 5. — A Weibull distribution of T_b, where the area under the curve represents the probability of failure within a tensile strength interval.

roughly describes the tensile strength around where many failures are occurring. It is also known as the characteristic life and is the T_b at which 63.2% of the tensile bars have failed, a proportion that is a characteristic of the Weibull distribution (the point where the proportion under the curve to the left of that point is 0.632). The β parameter roughly describes the slope of failures once failures occur. A positive β indicates failure is more likely over increasing tensile strength levels. The higher the β, the narrower the T_b range where failures occur. Ideally, our material will have a high α and β, indicating failure starts occurring at high T_b levels and failures occur within a small range. Because the true α and β parameters are unknown, we must estimate them by sampling from the material population. A population is comprised of all members of a group with true, but unknown characteristics. To estimate the characteristics of our material, we test a finite subset, a sample, from that population and use the sample measurements to estimate the true population characteristics. For the Weibull distribution, those characteristics are α and β.

RESULTS AND DISCUSSION

DISPERSION OF IS FROM XCT

The two polymeric IS materials considered in this study are labeled sulfur A and sulfur B of differing dispersibility corresponding to Crystex™ materials manufactured by Eastman Chemical Company as shown in Figure 7. A larger agglomeration of particles was observed for sulfur B than the agglomerated particles of sulfur, as shown in the SEM micrographs (Figure 7). Furthermore, the

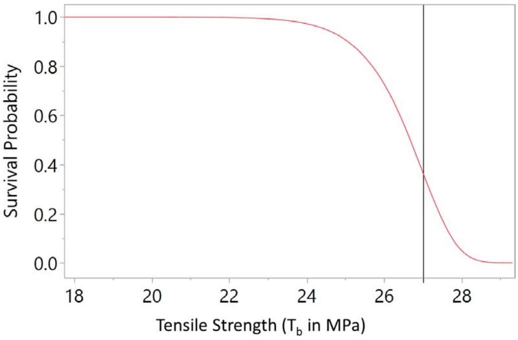

FIG. 6. — Survival plot of a Weibull distribution with $\alpha=27$ and $\beta=30$, illustrating probability of survival across T_b values.

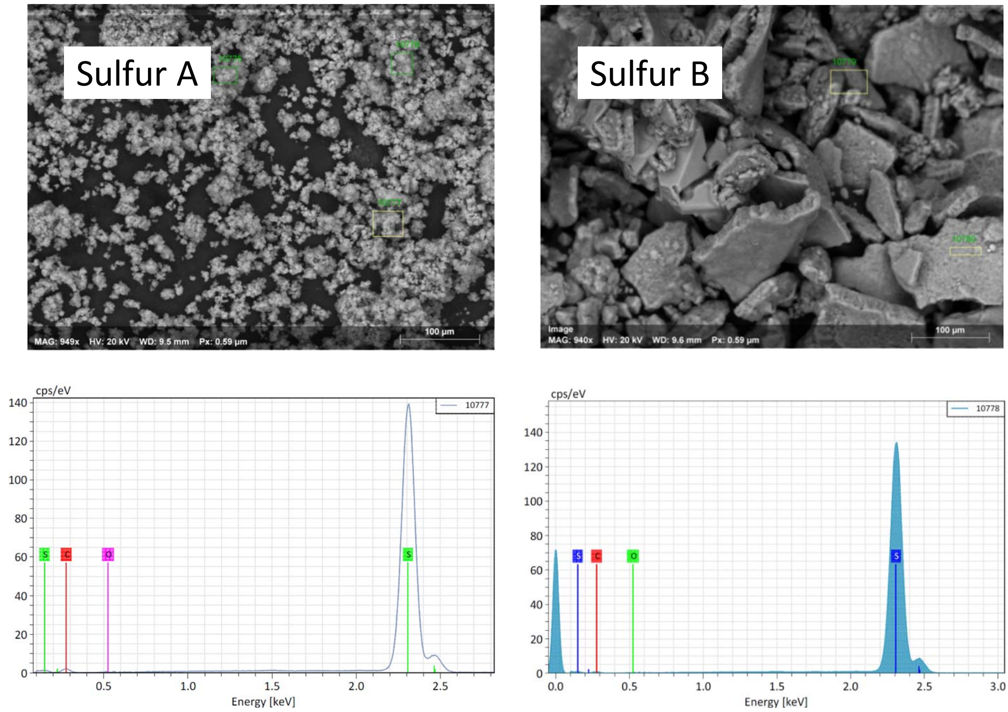

FIG. 7. — SEM Images of two sulfurs (labeled Crystex sulfur A and sulfur B) at similar magnification and corresponding energy X-ray dispersive spectra.

distribution of oxygen and two sulfur constituents peaks were observed for both sulfur materials by using EDS. The carbon peaks shown in the EDS spectra are from a conductive carbon tape used to mount the sulfur materials onto an SEM metal substrate. Sulfur B has inherently faster dispersion than sulfur A. Mixing energy sufficient to provide adequate dispersion for sulfur B should result in lower extent of dispersion for sulfur A, which should be apparent in the XCT and to some extent in a higher observed particle surface area by the optical microscopy technique with sulfur B, manifesting higher tensile properties.

Figure 8 shows the attenuation coefficients in each of the additives within the rubber compounds and shows a line profile through these powder-based materials, which are not fully consolidated, so considering partial void effects. It is clear that the XCT conditions corresponding to the peak energy of photons used for acquiring images and related current provide a clear distinction of each of these phases for quantitative analysis. Figure 9 shows two reconstructed slices of the material system by using 10 and 15 µm voxel size, and for the same sample at approximately similar location but obtained by two different operators to evaluate the repeatability of the measurement procedure. A preliminary conclusion is that highly repeatable data and related quantitative measurements are obtained with the established procedures used in this project.[24,42] The white particles correspond to sulfur, and gray matrix phase is the MB rubber compound. Such detailed information is now readily available along the height of the sample for evaluating the dispersion of a given sulfur type and manufacturing process steps involved in mixing and compounding processes.

The 3D distribution of the two types of sulfur particles is shown in Figure 10. It is clear that the dispersion of sulfur B is superior compared with sulfur A; thus, the probability of uniform distribution of crosslink density resulting from vulcanization step is much higher for rubber

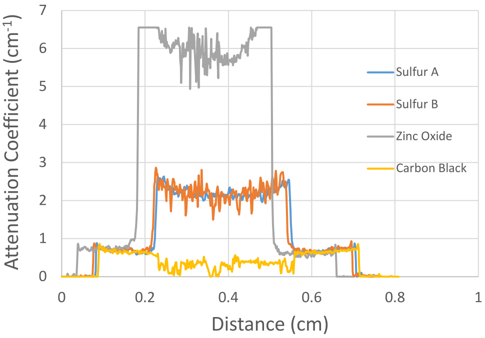

FIG. 8. — X-ray attenuation coefficients along line profiles consider partial volume effects for sulfur and other additives in the rubber compounds.

compounds with sulfur B. In addition to having the ability to qualitatively visualize both the dispersion and particle/agglomerate morphology from Figure 10, detailed quantitative analysis from the tomography data set can now de conducted. Figure 11 shows particle number distribution for sulfur particles whose volume is larger than 100 μm × 100 μm × 100 μm (or 0.001 mm^3). From Figure 11, it is conclusively interpreted that the dispersion of sulfur B versus sulfur A for particles having a volume larger than 0.001 mm^3 is superior. Corresponding volumetric size distribution indicates that the sulfur B has fewer particles larger than 100 μm considering an equivalent cube for the same volume of sample prepared under identical conditions and thus will have less chance of fatigue or fracture initiation sites corresponding to improved mechanical performance in terms of

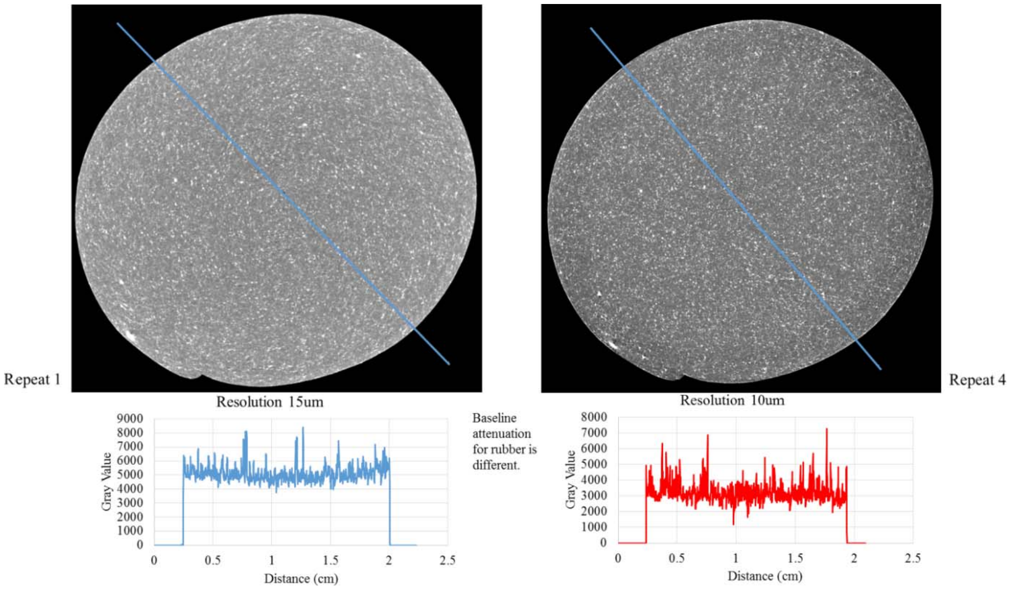

FIG. 9. — Effect of voxel size and repeatability: reconstructed slice at similar location along the height of the button type rubber compound at two resolutions. The bright spots correspond largely to sulfur particles, showing relative dispersion. The really bright agglomerates at few locations corresponds to zinc oxide particles (see bottom left periphery for example in this slice).

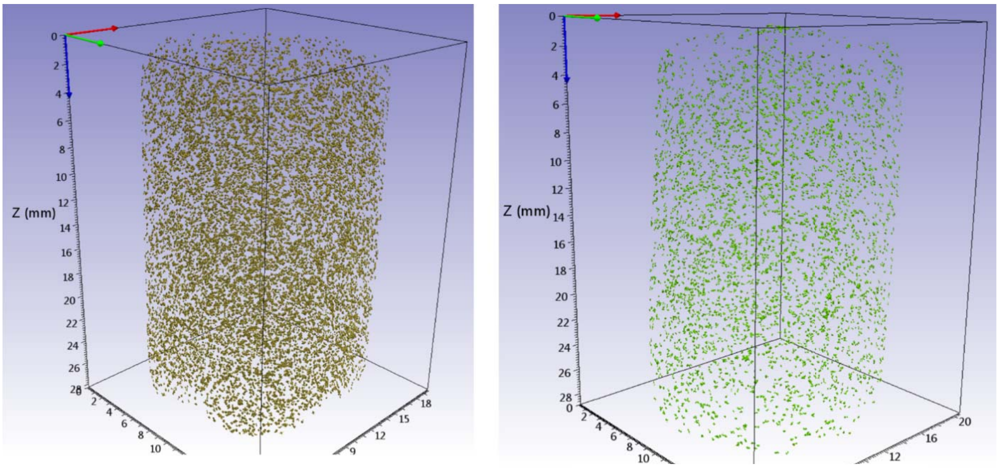

Compounded with Sulfur A Compounded with Sulfur B

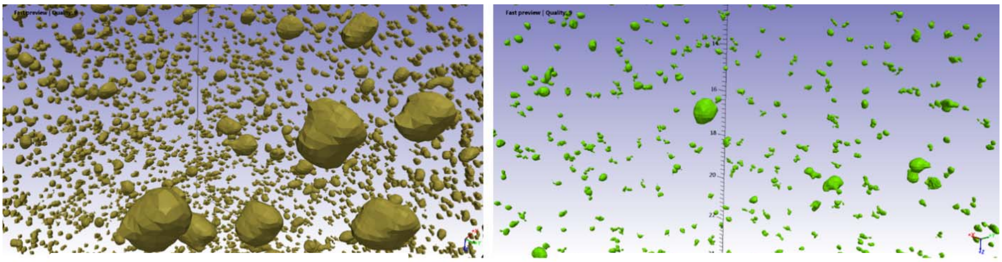

Compounded with Sulfur A Compounded with Sulfur B

FIG. 10. — 3D distribution of sulfur particles (Crystex sulfur A 13 vs sulfur B) whose size is greater than 100 μm cube and particle morphology from quantitative XCT data analysis. Each sample data contains approximately billion voxels for analysis and requires special computing resources for obtaining data shown here.

Weibull T_b and shape parameters after vulcanization. Because the progress in the field of rubber crosslinking has been remarkable in the past century, ongoing directions of research including silica-reinforced NR compounds, radiation and ultrasonic crosslinking, and the non-invasive characterization technique demonstrated herein are expected to have wide applications in these developments as well.[43]

DISPERSION CHARACTERIZATION VIA OPTICAL MICROSCOPY

The 2D optical images of the same rubber samples compounded using sulfur A and sulfur B are compared in Figure 12. Visual comparison does show clear differences between the two compounded sulfur samples qualitatively. These stitched images represent 32 cm^2 of rubber surface.

Numerical analysis of the contrast images provides the following population histograms (Figure 13) of the distribution of apparent particles in the images along with the particle population information. This represents a single-image comparison and to truly provide quantitative analytical distinction would require repeating multiple images.

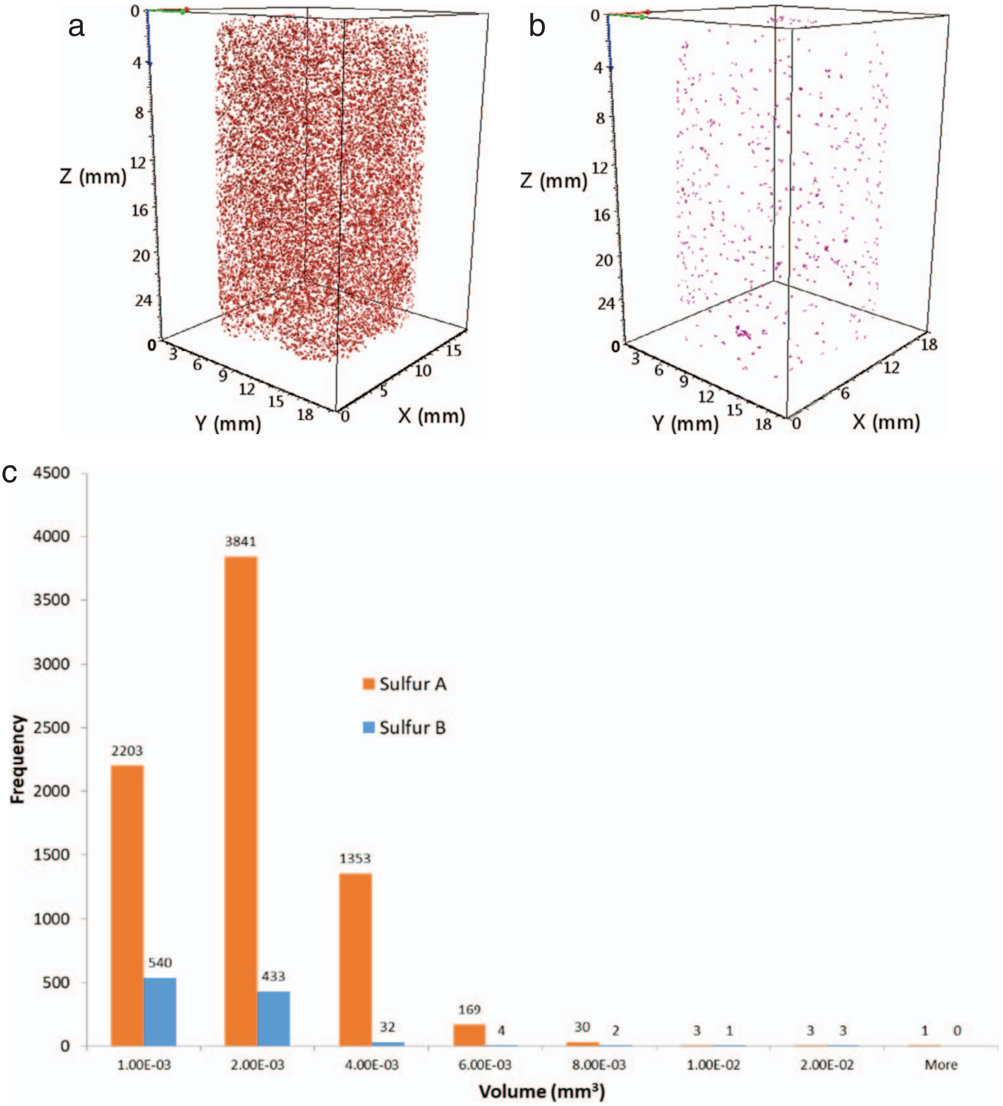

FIG. 11. — Dispersion of (a) sulfur A vs (b) sulfur B for particles having a volume larger than 0.001 mm^3 and (c) corresponding volumetric size distribution. Sulfur B has fewer particles larger than 100 μm, considering an equivalent cube, and thus will have less chance of fatigue or fracture initiation sites corresponding to improved mechanical performance in terms of Weibull strength and shape parameters.

TENSILE DISPERSION TESTING RESULTS

Looking at the large particles greater than 200 μm by optical imaging, sulfur A has significantly higher numbers of particles that contribute a higher percentage of observed particle area, as shown in Table IV. The rubber compound containing sulfur A is shown to have approximately an order of magnitude higher level of large particles present by the imaging analysis. The presumption in using the optical imaging technique is that these observable differences should be ascribed only to the differences in the dispersibility of the two sulfur materials. Because the mixer used the same MB, zinc oxide, and accelerator, any difference logically stems from differences in the sulfur products.

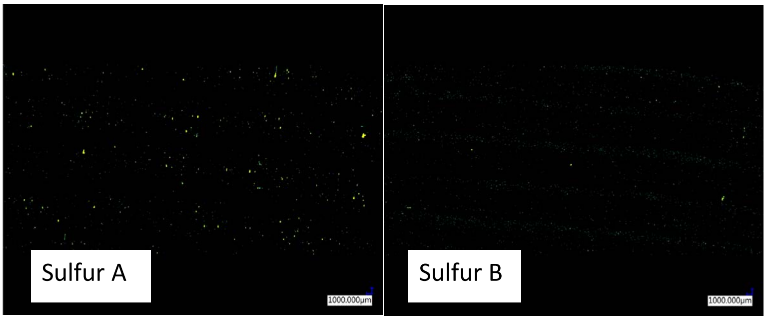

FIG. 12. — Optical contrast image of compounded rubber using sulfur A and sulfur B.

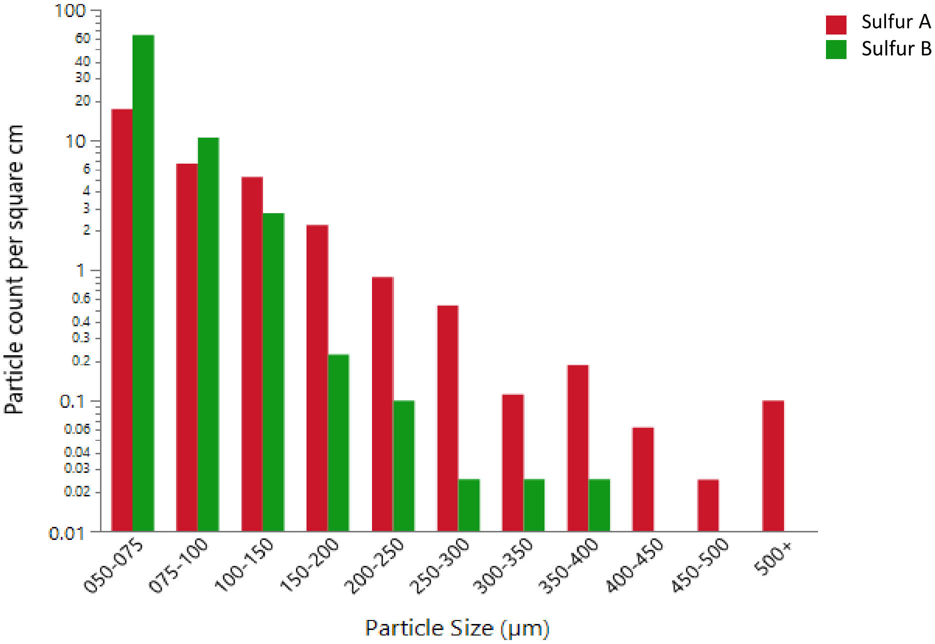

FIG. 13. — Histogram comparing optical image of sulfur A and sulfur B compounded rubber.

TABLE IV
ABSOLUTE AND RELATIVE PARTICLE COUNTS FOR PARTICLES WITH DIAMETERS >200 μm

	Particle count >200 μm per image	% of surface area attributed to particles >200 μm
Sulfur A	77	0.159
Sulfur B	7	0.011

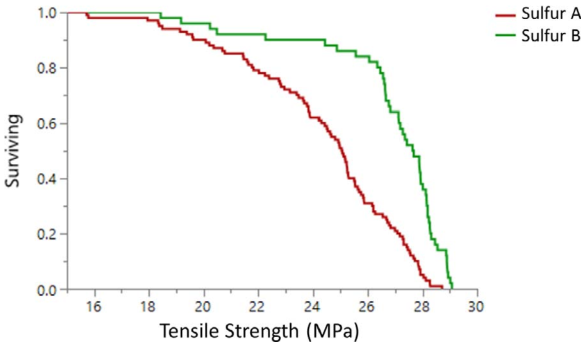

FIG. 14. — Tensile survival plot comparing the dispersibility of sulfur A and sulfur B compounded rubber.

The shortcoming of this technique, of course, stems from the inability to ascribe the origin of the particles.

Tensile dispersion results reflect the inherent critical flaw population distribution (Figure 14) from all sources. Although this is a great analysis for a production situation informing about the quality of the mix of all ingredients, again it must be considered an indirect technique because tensile variance arises from any critical flaw. Because the same MB, accelerator, and zinc oxide are used in both mixes, the differences would be potentially ascribable to the differences in the dispersion of the two sulfur products. This is exhibited in both the calculated Weibull α and β values shown in Table V. The lower reported Weibull values listed for sulfur A reflect a lower strength to failure (in megapascals) for Weibull α and larger variance for Weibull β.

CONCLUSIONS

Dispersion of insoluble sulfur and an experimental procedure for obtaining non-invasive quantitative analysis of additives in rubber compounds is demonstrated using laboratory-based X-ray computed tomography (XCT). Digital XCT was performed using a custom-developed laboratory micro-focus–based source (maximum energy of 130 KeV with fine spot size of 5 μm) and a high resolution and efficiency scintillator–based flat panel detector by using cone beam optics. This method is conducive to adaption of currently used optical microscopy techniques where microstructure for such elastomeric materials is obtained by destructive techniques such as sectioning of samples, subsequent careful polishing in some instances, obtaining two-dimensional images from optimal microscopy followed by digital image analysis. The main difference here being the microstructure is obtained non-invasively based on attenuation contrast of the additives compared with each other (e.g., insoluble sulfur versus zinc oxide particles) and with the matrix phase (NR with carbon black and other polymers). The three-dimensional distribution of the two types of sulfur particles for identically prepared rubber

TABLE V
WEIBULL α AND β CALCULATED PARAMETERS FROM TENSILE DISPERSION TESTING

	Weibull α	Weibull β
Sulfur A	25.5	12.6
Sulfur B	27.7	18.9

compounds is presented and shows that the dispersion of sulfur B is superior to that of sulfur A. Thus, the probability of uniform distribution of crosslink density resulting from post-vulcanization step is much higher for rubber compounds with sulfur B; insoluble sulfur and mechanical property distributions resulting for these two insoluble sulfurs are also included as a correlation with mechanical properties. In addition, the ability to qualitatively visualize both the dispersion and particle/agglomerate morphology are quantified in terms of particle size distribution considering its volume specifically for sulfur. Comparative results of dispersion analysis via optical imaging technique and tensile dispersion are in general agreement with the data afforded by the high-resolution sulfur contrast technique using light microscope images technique, but without the specificity inherent by high-resolution XCT.

ACKNOWLEDGEMENTS

Research resulted from a program managed by Kate Kornau, Eastman External Innovation Manager, and the financial support is gratefully acknowledged by Penumadu from the University of Tennessee, Knoxville. Technical support of John Dunlap and James Eun from the University of Tennessee, Knoxville, is gratefully acknowledged.

REFERENCES

[1] W. V. Mars and A. Fatemi, *Int. J. Fatigue* **24**, 949 (2002).

[2] C. G. Robertson, L. B. Tunnicliffe, L. Maciag, M. A. Bauman, K. Miller, C. R. Herd, and W. V. Mars, *Polymer* **12**, 203 (2020).

[3] F. Li, J. Liu, W. V. Mars, T. W. Chan, Y. Lu, H. Yang, and L. Zhang, *Int. J. Fatigue* **80**, 50 (2015).

[4] C. G. Robertson and N. J. Hardman, *Polymer* **13**, 538 (2021).

[5] G. S. Fielding-Russell and R. L. Rongone, *Polymer* **56**, 838 (1983).

[6] B. Huneau, I. Masquelier, Y. Marco, V. Le Saux, S. Noizet, C. Schiel, and P. Charrier, RUBBER CHEM. TECHNOL. **89**, 126 (2016).

[7] N. Tabsan, S. Wirasate, and K. Suchiva, *Wear* **269**, 394 (2010).

[8] M. Wang, J. Zhu, S. Zhang, G. You, and S. Wu, *Polym. Test.* **80**, 106145 (2019).

[9] A. Susanna, L. Armelao, E. Callone, S. Diré, M. D'Arienzo, B. Di Credico, L. Giannini, T. Hanel, F. Morazzoni, and R. Scotti, *Chem. Eng. J.* **275**, 245 (2015).

[10] G. Heideman, R. N. Datta, J. W. N. Noordermeer, and B. van Baarle, *J. Appl. Polym. Sci.* **95**, 1388 (2005).

[11] *The Mixing of Rubber*, R. F. Grossman, Ed., Chapman & Hall, Dordrecht, The Netherlands, 1997.

[12] L. Chen, Z. Jia, X. Guo, B. Zhong, Y. Chen, Y. Luo, and D. Jia, *Chem. Eng. J.* **336**, 748 (2018).

[13] A. Dong, Z. Zhang, J. Haixiang, S. Jinquan, Z. Huan, and L. Yaqing, RUBBER CHEM. TECHNOL. **90**, 611 (2017).

[14] N. D. Bansod, B. P. Kapgate, P. K. Maji, A. Bandyopadhyay, and C. Das, RUBBER CHEM. TECHNOL. **92**, 219 (2019).

[15] B. P. Kapgate, C. Das, D. Basu, A. Das, and G. Heinrich, *J. Elast. Plast.* **47**, 248 (2015).

[16] S. Prasertsri and N. Rattanasom, *Polym. Test.* **30**, 515 (2011).

[17] D. H. C. Wong, A. Childress, and F. Ignatz-Hoover, "Evaluation of Sulfur Dispersion Using Population Survival Analysis," in Proceedings of 13th Fall Rubber Colloquium, November 6–8, 2018, Hannover, Germany.

[18] F. Ignatz-Hoover, A. R. Katritzky, V. S. Lobanov, and M. Karelson, RUBBER CHEM. TECHNOL. **72**, 318 (1999).

[19] L. Chen, W. Zhou, J. Lu, J. Li, W. Zhang, N. Huang, L. Wu, and L. Li, *Macromolecules* **48**, 7923 (2015).

[20] F. Ignatz-Hoover and B. H. To, *Rubber World*, November, 2010, pp 21–26.

[21] *Engineering with Rubber: How to Design Rubber Components*, 2nd Edition, Alan Gent, Ed., Rubber Division of the American Chemical Society, Hanser Publishers, Cincinnati, Ohio, 2001.

[22] S. Robin and T. Alshuth, “Lifetime Prediction—A Unification of the Fracture Mechanics and the Wöhler Concept, ” in Constitutive Models for Rubber VIII, in Proceedings of the 8th European Conference on Constitutive Models for Rubber, San Sebastian, Spain, June 25–28, 2013, pp 405–407.

[23] M. Ludwig, C. Robertson, F. Ignatz-Hoover, S. Basu, and T. Alshuth, “Micro/Nano CT–A Useful Tool for the Characterization of Silica Dispersion,” in Proceedings International Rubber Conference/Deutsche Kautschuk Tagung (DKT) June 29–July 2, 2015, Nuremburg, Germany.

[24] “Simpleware: Converting 3D Images into Models Reference Guide Version 2016.09,” Synopsys, Inc., 2016.

[25] D. Penumadu, F. Kim, and J. Bunn, *J. Exp. Mech.* **56**, 607 (2016).

[26] ASTM Standard D 623-07, “Standard Test Method for Rubber Property – Heat Generation and Flexing Fatigue in Compression,” *Annu. Book ASTM Stand.* **9.01**, 1 (2014).

[27] W. M. Hess, RUBBER CHEM. TECHNOL. **64**, 386 (1991).

[28] B. M. Patterson, N. L. Cordes, K. Henderson, J. C. E. Mertens, A. J. Clarke, B. Hornberger, A. Merkle, S. Etchin, A. Tkachuk, M. Leibowitz, D. Trapp, W. Qiu, B. Zhang, H. Bale, X. Lu, R. Hartwell, P. J. Withers, and R. S. Bradley, *Exp. Mech.* **56**, 1585 (2016).

[29] T. Watanabe, Y. Takeichi, Y. Niwa, M. Hojo, and M. Kimura, *Compos. Sci. Technol.* **197**, 108244 (2020).

[30] Y. Wang, Y. Ren, G. Zhou, G. Du, H. Xie, B. Deng, and T. Xiao, *Nucl. Instrum. Methods Phys. Res. A* **896**, 108 (2018).

[31] H. Rolland, N. Saintier, P. Wilson, J. Merzeau, and G. Robert, *Compos. B. Eng.* **109**, 170 (2017).

[32] R. Böhm, J. Stiller, T. Behnisch, M. Zscheyge, R. Protz, S. Radloff, M. Gude, and W. Hufenbach, *Compos. Sci. Technol.* **110**, 62 (2015).

[33] K. Le Gorju Jago, RUBBER CHEM. TECHNOL. **85**, 387 (2012).

[34] *Principles of Computerized Tomographic Imaging*, R.E. O’Malley, Ed., Society for Industrial and Applied Mathematics, Philadelphia, Pennsylvania, 2001.

[35] Y. De Witte, J. Vlassenbroeck, and L.V. Hoorebeke, *IEEE T Image Process* **19**, 2419 (2010).

[36] “Octopus Reconstruction User Manual, Version 8.9.2,” Inside Matters, 2016.

[37] J. Vlassenbroeck, M. Dierick, B. Masschaele, V. Cnudde, L. Van Hoorebeke, and P. Jacobs, *Nucl. Instrum. Methods Phys. Res. A* **580**, 442 (2007).

[38] L. A. Feldkamp, L. Davis, and J. Kress, *J. Opt. Soc. Am.* **1**, 612 (1984).

[39] R. Sakin and I. Ay, *J. Mater. Des.* **29**, 1170 (2007).

[40] H. P. Zhu, X. Xia, C. H. Yu, A. Adnan, S. F. Liu, and Y. K. Du, *BMC Gastroenterol.* **11**, 1 (2011).

[41] C. Liu, A. Eser, T. Albrecht, V. Stournari, M. Felder, S. Heintze, and C. Broeckmann, *Dent. Mater. J.* **37**, 94 (2021).

[42] G. Melenka, E. Lepp, B. K. O. Cheung, and J. P. Carey, *J. Compos. Struct.* **131**, 384 (2015).

[43] M. Akiba and A. S. Hashim, *Prog. Polym. Sci.* **22**, 475 (1997).

[*Received January 2020, Revised April 2021*]